Dual-Electrodynamic Wheel Force Analysis

Colton Bruce, Jonathan Z. Bird, Matthew Grubbs

Laboratory for Magnetomechanical Energy Conversion and Control Portland State University, Department of Electrical and Computer Engineering, Portland, OR, USA

The rotation of an electrodynamic wheel (EDW) above a flat conductive, non-magnetic, track induces currents in the track that can create lift and thrust/braking force. This paper presents a new type of dual-EDW that consists of two EDWs in series that can also create a controllable lateral force. The magnitude and direction of the lateral force can be changed via the relative phase angle shifting of the two rotors. The changes in the lateral force magnitude as well as direction are shown to not affect the lift and thrust force magnitude. The geometric analysis of the design is presented and the practical difficulty of implementing the design is also discussed.

Index Terms— Eddy current, electrodynamic wheel, finite element analysis, magnetic levitation.

I. INTRODUCTION

A SELECTRODYNAMIC wheel (EDW) creates lift and thrust force through the rotation of a magnetic rotor above a passive conductive track, made of aluminum or copper [1-7]. EDWs are being studied for use in magnetic levitation (maglev) vehicles, and recently a four wheeled [5, 6] and six wheeled [7] EDW-maglev prototype vehicle has been designed. As the flat track is passive the use of an EDW could enable the maglev levitation (maglev) infrastructure to be as low cost as alternative high-speed rail systems. A flat track guideway also could enable the EDW-maglev vehicle to be integrated into existing rail and highway infrastructure.

Due to the edge-effects the rotation of a radial EDW over a finite-width flat track will create lateral instability [5]. One approach to creating lateral recentering force is to use a split-sheet track design [2], however the re-centering force created by the split-track is relatively small and the lateral forces do not scale well as the size increases. In addition, a split in the track greatly reduces the lift-to-weight ratio and thrust force [2]. A second option that has been proposed in the past is to use active control to rotate the EDWs around a vertical axis [1]. By mechanically rotating the orientation of the wheels the angle of the translational force is controlled and therefore the lateral position is shifted. However, this method introduces relatively significant mechanical design complexities and does not provide passive stability during lateral disturbances.

Recently the use of a vertical conductive sheet side-wall with an EDW has been shown to provide a sizable eddy current induced recentering force, the side-wall also increases the lift and thrust force [5]. But using a conductive side wall will increase the guideway complexity.

This paper investigates the forces created by a new dual-EDW design, as shown in Fig. 1, that can create lateral recentering force when using a completely flat conductive track. The dual-EDW configuration contains a front-EDW with a one pole-pair diametrically magnetized rotor, and a rear-EDW that contains two 180-degree phase shifted one pole-pair diametric magnetized rotor magnets. The rear-EDW magnets are magnetization anti-parallel with each other, thereby creating a transverse directed pole-pair. Unless otherwise specified the axial offset length l_m as defined in Fig. 1(b) is assumed to be zero, this is the ideal case.

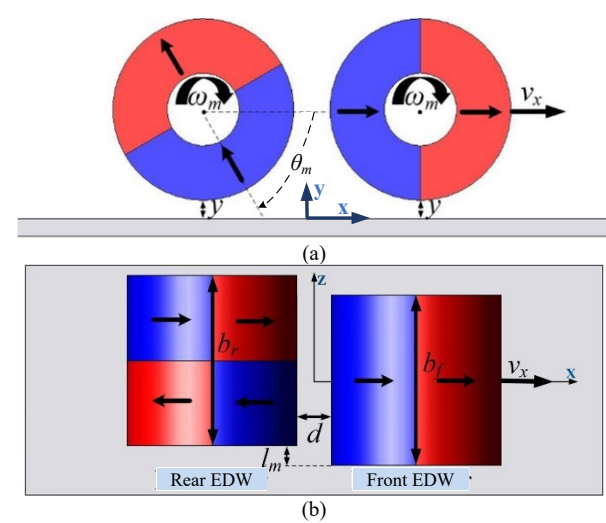


Fig. 1. (a) Side-view of the dual-EDW that are separated by a distance, d and the front-EDW and rear-EDW have equal width, $b_f = b_r$. (b) shows a top-view (when $\theta_m = 0$) also shown is an axial offset misalignment, l_m .

This paper uses an analytic-based 3-D second order vector potential (SOVP) steady-state model to compute the forces and rotor torque [3, 4]. This analytic-based model is used to determine the geometric parameters that help to maximize the lateral force. A discussion of the practical difficulties of implementing the new design is also presented.

II. FORCE ANALYSIS

Assuming an absence of track edge-effects, then if the rear-EDW was by itself, it would create a net-zero lateral force. Regardless of the orientation of the single rotor, the eddy current forces produced on each half of the magnet rotor will be such that the forces are directed to push the magnet in the direction of that half of the magnet, relative to the axial center. The equal and opposite lateral forces will always cancel out. However, with the addition of the front-EDW, the presence of the rear rotor alongside the single pole-pair front rotor causes a relative change in field variation experienced by the conducting track, with the fields on one axial half of the EDW constructively adding, and the other half destructively adding. This results in a relative increase in the induced current in the track, and thus the reflected magnetic field, on one side of the EDW, and a relative reduction in induced current on the other side of the EDW. The

interaction between the EDW fields and the axially imbalanced induced track fields causes an imbalanced lateral force to be created, giving rise to a non-zero lateral force.

A. Force Validation

Due to the need to simultaneously model high-speed rotational and translational motion in 3-D the use of a finite element analysis (FEA) eddy current solver is computationally challenging. Therefore, an analytic-based (SOVP) steady-state 3-D eddy current model developed by Paul *et al.* [3, 4] was used. The derivation of the dual-EDW model is summarized in the Appendix. Using the values shown in Table I this model was validated by comparing it with a 3-D JMAG FEA model. An example force comparison is shown in Fig. 2. Fig. 2(a) compares the lateral force as a function of phase angle, and Fig. 2(b) compares the lift and thrust force values. The phase angle θ_m is defined in Fig. 1(a). A very good agreement between the analytic and FEA is seen. The lateral force is sinusoidal and a function of θ_m , but interestingly the lift and thrust force are not affected by changes in phase angle.

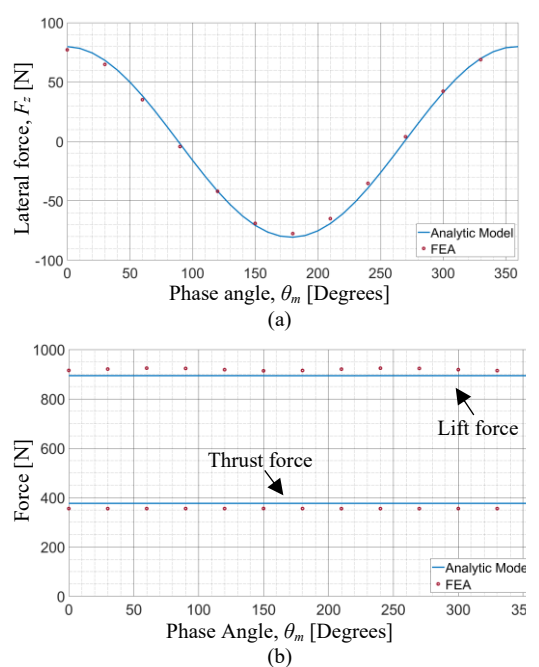


Fig. 2. Dual-rotor EDW analytic model and FEA model phase angle change force comparison for (a) lateral force and (b) lift and thrust force. Parameters used are as given in Table I. The rotors angular speed and translational speed were fixed at $(\omega_m, v_x) = (1000 \text{ r/min}, 0 \text{ m/s})$.

TABLE I. DUAL- EDW MODEL PARAMETERS

| Rotor | Value | Units |
|------------------------------|--------------------|------------------|
| Magnet residual flux density | 1.42 T | T |
| Magnet relative permeability | 1.055 | - |
| Airgap, y_g | 10 | mm |
| Outer Radius, r_o | 50 | mm |
| Inner Radius, r_i | 10 | mm |
| Rear rotor width, b_r | 100 | mm |
| Front rotor width, b_f | 100 | mm |
| Rotor offset, d | $0.1r_{\rm o}$ | mm |
| Axial offset length, l_m | 0 | mm |
| Track conductivity, σ (Cu) | 5.69×10^7 | Sm ⁻¹ |
| Track thickness, h | 12.7 | mm |

III. PHASE ANGLE AND SLIP SPEED

The phase angle that results in the peak force and zero force operating point is not constant, but changes with the translational velocity and the slip, where the slip speed is defined by

$$s = \omega r_o - v_x \tag{1}$$

and ω = angular speed, v_x = translational speed, and r_o = outer rotor radius. As an example, Fig. 3 shows how the peak lateral force phase angle is shifted with slip when $v_x = 25$ m/s, this is in addition to the peak force changing. The changes in force magnitude and angle are shown in Fig. 4, in which the peak positive, lateral force and the phase angle that results in this force was evaluated. The peak lateral force occurs near zero slip and its peak value is comparable to that of the thrust force indicating it should scale well. Fig. 4 shows that there is a maximum peak operating slip, with the achievable lateral force decreasing as the operating point diverges from this value, leveling out to a near constant value at very high slip. The peak force phase angle ranges between -50° to 180° and since the maximum negative and positive force values are 180° apart, the variation in peak force phase angle can be significant enough to flip over the possible range of operations.

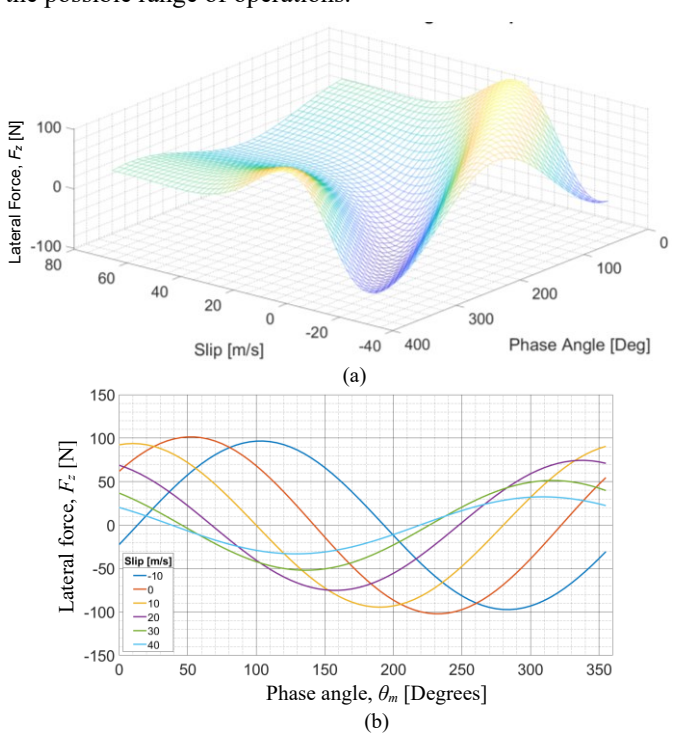


Fig. 3. Lateral force vs phase angle plot for different slip speeds, s, values when the translational velocity is $v_x = 25$ m/s. The peak lateral force phase angle depends on the slip value.

IV. SCALING CHARACTERISTICS

In the following study the geometric factors that influence the dual-EDW forces are studied using the 3-D steady-state SOVP dual-rotor model that is presented in the Appendix.

A. Rotor Spacing

The dual-EDW fields are a superposition of the rear rotors transverse pole-pair and front rotors' single pole-pair. A lateral force is produced because of the imbalance in the axial field variation. Therefore, the spacing, *d*, between the rotors must

play a large role in the range of lateral forces that can be created. To study the relative effect of rotor spacing a rotor spacing ratio, defined as

$$\Gamma = d / r_{o}. \tag{2}$$

has been used. As the rotor spacing ratio increases, the influence of the two rotors on each other declines, decreasing the generated lateral force. This occurrence can be seen in Fig. 5, in which the values shown in Table I were used to plot the peak lateral force as a function of the rotor spacing ratio. Fig. 5 shows that the smallest practical spacing d between rotors should always be selected.

The thrust and lift forces are also shown Fig. 5 and interestingly the forces are constant with rotor offset ratio. This is because there is an unequal lift and thrust force on each axial side of the rotor. Due to the rotor field interactions, one side results in a decrease in force relative to that produced when the rotors are independent of each other. But the other side resulting in an increase in force. Unlike the lateral force, however, the thrust and lift forces on each side of the rotors have the same direction, and thus the forces always add constructively. As the rotor spacing changes, the increase and decrease in the forces on either side of the rotors varies, but in equal amount, resulting in a net force that is constant. This is not the case if the rear rotor contained a single magnet pole-pair across the entire width.

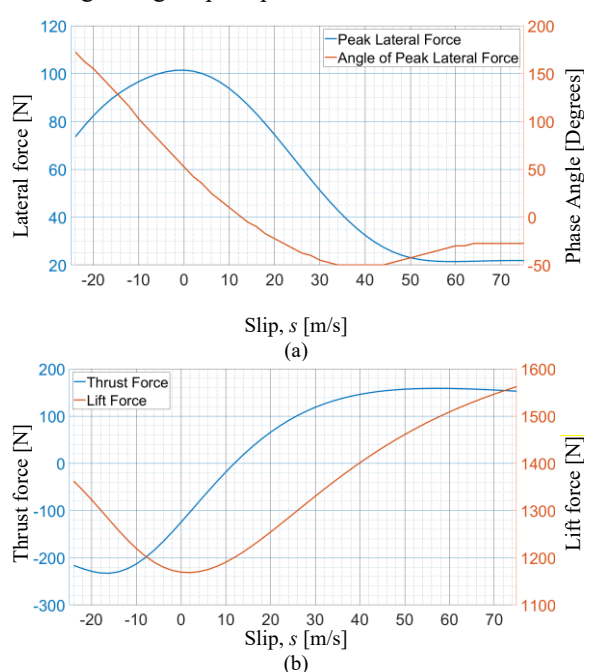


Fig. 4. (a) Peak lateral force as a function of slip speed and the associated phase angle for the dual-rotor EDW, (b) the change in thrust and lift force as a function of slip.

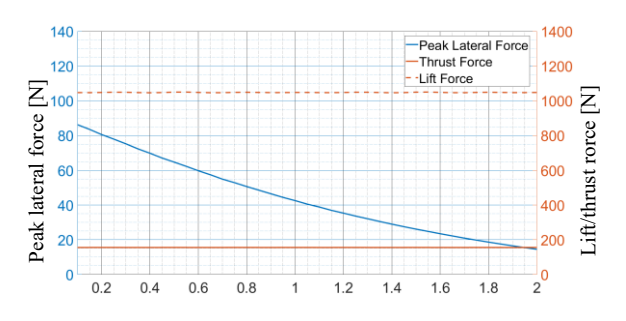
B. Rotor Width

The relative rotor width plays a significant role in the magnitudes of force produced by the dual-EDW. If the EDWs do not have the same width, then this will limit the region that the fields from each rotor can meaningfully interact. This influence was studied by using a front and rear-rotor width factor, defined respectively by

$$\Lambda_f = b_f / r_o \tag{3}$$

$$\Lambda_r = b_r / r_o . {4}$$

Fig. 6 shows how the forces change as a function of the rear rotor width ratio Λ_r for the case when $\Gamma=0.1r_0$ and when the front rotor has a fixed width ratio of $\Lambda_f=2$. Fig. 6 shows that as the rear rotor width increases, the peak lateral force initially increases rapidly, then begins to level out, approaching a constant value at a higher rear rotor width. Therefore, it is recommended that by selecting a rear rotor that is double the axial width of the front rotor, such that $\Lambda_r=2\Lambda_f$, a lateral force that is ~78 % of the peak force will be obtained. Further size increases have a diminishing return.



Rotor spacing ratio, Γ [-] Fig. 5. Dual-rotor EDW lateral force, thrust force and lift force as a function of rotor offset ratio when $(s, v_x) = (10,10)$ m/s. Except as noted, parameters are as given in Table I.

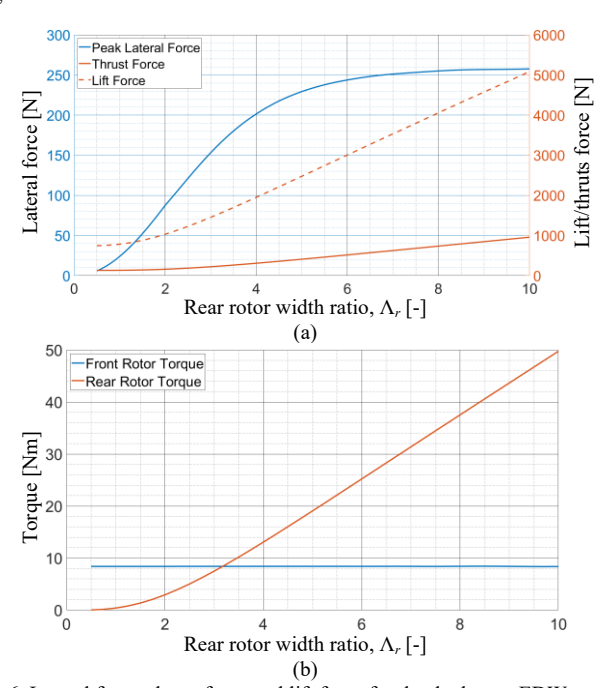


Fig. 6. Lateral force, thrust force and lift force for the dual rotor EDW as a function of rotor width ratio when the front rotor width is fixed at $\Lambda_f = 2$. $(s, v_x) = (10 \text{ m/s}, 10 \text{ m/s})$. (b) shows the torque requirement for the front and rear rotor. Except as noted, the parameters are as given in Table I.

IV. PRACTICAL IMPLEMENTATION

When the two diametrically magnetized one pole rotors are in close proximity they will give rise to a large sinusoidal torque [8]. As the rear-EDW magnets are magnetization antiparallel with each other, their 180° phase shift eliminates the magnet rotor torque. To demonstrate this internal torque elimination the proof-of-principle dual-EDW design, as shown in

Fig. 7 was constructed. The construction demonstrated the practical difficulties in implementing the presented design. To eliminate the internal force between the magnets the mechanical alignment needed to be extremely precise along with the magnetization alignment. For instance, Fig. 8 shows that even a small misalignment in the axial position l_m will give rise to a sizable magnet rotor torque. Fig. 8 also shows that just a 5° error difference in the rotor magnetization misalignment will also results in a significant magnet rotor interaction torque. These practical factors made constructing and successfully testing the prototype challenging.

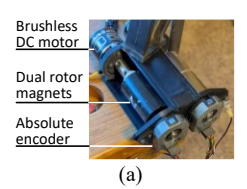




Fig. 7. (a) Side-view and (b) top-view (when $\theta_m = 0$) for a dual-rotor EDW. The rotor radii are $r_o = 12.7$ mm and the front rotor has a width $b_f = 40$ and the rear rotor has a width $b_r = 50.8$ mm.

V. FINITE WIDTH FORCE ANALYSIS

The dual-EDW lateral force can be used to counteract the finite-width edge-effect destabilization force. As an example, consider the design shown in Fig. 9, in which the track width is $w_t = 200$ mm, and the rotor width is $b_r = b_f = 100$ mm. The remaining model parameters are as given in Table I. The lateral force created by the dual-EDW was computed, using JMAG 3-D FEA, to be $F_{z,s} = -100$ N. Therefore, this is the maximum lateral force that can be created at the track center. Fig. 10 shows how the value of the net-lateral force changes as the dual-EDW moves off-center. The axial center is at $Z_o = 0$ as defined in Fig. 9. The lateral force plot in Fig. 10 shows that for $Z_o < 28$ mm a steady-state (average) negative force can be created that counteracts the edge-effect's de-stabilization force. However, as a force ripple exists the effective range of stabilization will be lower.

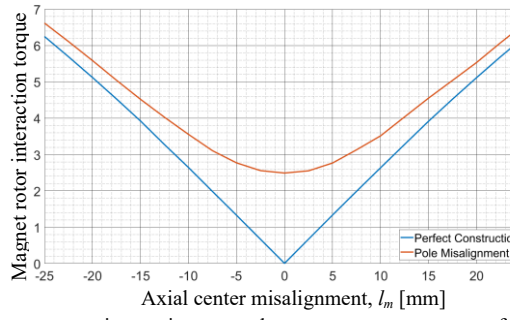


Fig. 8. Rotor magnet interaction torque between magnet rotors as a function of rear rotor axial center offset. Also shown is the torque when the magnetization vector has a 5° offset relative ideal. The parameters used are given in Table I. The analysis was completed for the case when $(\omega_m, v_x) = (1000 \text{ r/min}, 25 \text{ m/s})$.

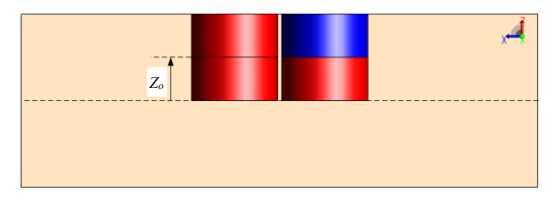


Fig. 9. Top view of the FEA model for the dual-rotor EDW. When the axial position $Z_o = 0$ the rotors will be centered over the track.

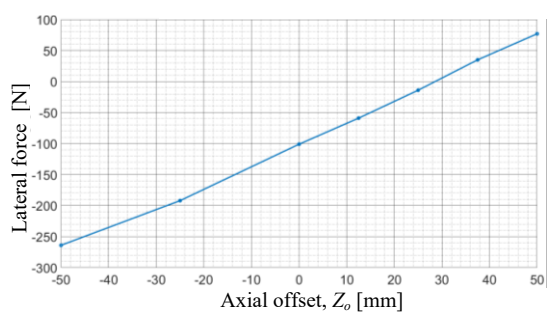


Fig. 10. Lateral force as a function of axial offset. The model uses the parameters shown in Table I. The EDW was rotated at $\omega=1000$ r/min.

It should be noted that the size of the lateral force can be increased further by using a third EDW in series, like as shown in Fig. 11(a). In this case the blue magnets are all magnetized in the opposite diametric direction to the red magnets. The Fig. 11(a) configuration will ideally cancel out the internal torque and double the lateral force. It should be noted that the three-EDW design shown in Fig. 11(b) will not cancel out the internal torque and is therefore not advisable.

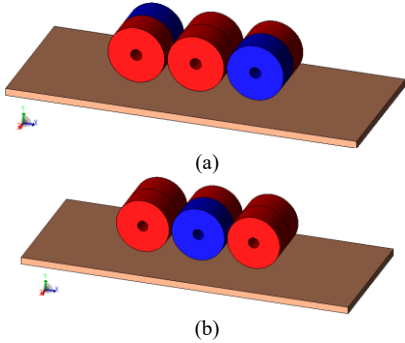


Fig. 11. Three-series EDW (a) contains that the one pole-pair transverse-flux rotor on the sides (b) contains a central transverse-flux rotor. The blue magnets are all magnetized in the opposite diametric direction to the red magnets.

CONCLUSIONS

This paper has presented a new type of dual-EDW design that can create lateral recentering force over a flat track. It is shown that the lateral force can be independently changed, through rotor phase angle shifting, and does not change the lift and thrust force. Ideally the dual-EDW should eliminate the internal magnet torque between the rotors. However, because of mechanical tolerance limitations and differences in magnet magnetization the complete elimination of the internal rotor torque is challenging to achieve in a practical design.

ACKNOWLEDGEMENTS

The authors would like to thank the JMAG Corporation for the use of their FEA software. This material is based upon work supported by the National Science Foundation under grant number 1810489.

APPENDIX

A. Dual-EDW Rotor Field

In [3, 4] it is shown that a magnetic rotor can be modeled by a cylindrical magnetic charge sheet along the surface of the magnet. Using this method, the magnetic flux density of a EDW rotor can be calculated by

$$\mathbf{B}(x, y, z) = \frac{1}{4\pi} \int_{0}^{2\pi} \int_{0}^{b/2} \frac{\rho_m(\theta_o, z_o)}{R^3} r_o \mathbf{R} dz_o d\theta_o$$
 (5)

where

$$\mathbf{R} = (x - r_o \cos \theta_o)\hat{x} + (y - r_o \sin \theta_o)\hat{y} + (z - z_o)\hat{z}$$
 (6)

 ρ_m is the magnetic charge density on the cylindrical charge sheet model of the rotor, r_o is the outer radius of the magnet. Applying Gauss's Law to the cylindrical charge surface, ρ_m is found to be equal to twice the component of the source magnet's flux density that is normal to the sheet [9]. Assuming the magnetization is uniform along the axial length, the front-EDW rotor's source charge density function can be expressed as:

$$\rho_{m,1}(\theta_o, z_o) = 2B_r^s(r_o, \theta_o) \left[u\left(z_o + b_f/2\right) - u\left(z_o - b_f/2\right) \right]$$
(7)

where u is a step function. For P = 1 pole-pairs the radial flux density component at the rotor surface can be approximated by [10]

$$B_n^s(r_o, \theta) = \frac{B_{rem}(1 + \mu_r) \left[r_o^2 - r_i^2 \right]}{\left[(1 - \mu_r)^2 r_i^2 - (1 + \mu_r)^2 r_o^2 \right]} \cos(\theta)$$
 (8)

where μ_r = magnet relative permeability, and B_{rem} = magnet remnant flux density of the rotor. The rear-EDW rotor can be modeled as two single rotors side by side, with one segment's magnetization 180° angularly shifted relative to the other. This lets the effective magnetic charge density to be given by

$$\rho_{m,2}(\theta_o, z_o) = 2B_n^s(r_o, \theta_o + \pi) \left[u(z_o + b_r/2) - u(z_o) \right]$$

$$+ 2B_n^s(r_o, \theta_o) \left[u(z_o) - u(z_o - b_r/2) \right]$$
(9)

Substituting (7), (8), and (9) into (5) the normal component of the magnetic flux density for the front and rear-EDW is

$$B_{y,f}(x,y,z) = \frac{r_o}{2\pi} \int_0^{2\pi} \frac{B_n^s(r_o,\theta_o)(y-r_o\sin\theta_o)}{r^2} \left[\frac{2z+b_f}{\sqrt{(2z+b_f)^2+4r^2}} \right]$$

$$-\frac{2z - b_f}{\sqrt{(2z - b_f)^2 + 4r^2}} \Bigg] d\theta_o (10)$$

$$B_{y,r}(x,y,z) = \frac{r_o}{2\pi} \int_{0}^{2\pi} \frac{(y - r_o \sin \theta_o)}{r^2} \left[B_n^s(r_o, \theta_o) \frac{z}{\sqrt{z^2 + r^2}} \right]$$

$$+B_{n}^{s}(r_{o},\theta_{o}+\pi)\frac{2z+b_{r}}{\sqrt{(2z+b_{r})^{2}+4r^{2}}}-B_{n}^{s}(r_{o},\theta_{o}+\pi)\frac{z}{\sqrt{z^{2}+r^{2}}}$$

$$-B_{n}^{s}(r_{o},\theta_{o})\frac{2z-b_{r}}{\sqrt{(2z-b_{r})^{2}+4r^{2}}}\Bigg]d\theta_{o} \quad (11)$$

where

$$r^{2} = (x - r_{o} \cos \theta_{o})^{2} + (y - r_{o} \sin \theta_{o})^{2}$$
 (12)

The total magnetic flux density is then

$$B_{v}^{so}(x, y, z) = B_{v, f}^{s}(x - [d/2 + r_o], y, z)$$

$$+B_{y,r}^{s}(x+(d/2+r_{o}),y,z)$$
 (13)

B. Eddy Current Force

The 3-D analytic based eddy current force equation for an EDW with a velocity v_x and angular speed ω is given by [3, 4]

$$\mathbf{F} = \frac{wl}{\mu_0} \operatorname{Re} \left\{ \sum_{m=-M}^{M} \sum_{n=-N}^{N} \left| S_{mn}^{y} \right|^2 e^{-2\kappa_{mn}y_g} R_{mn} \left[\frac{j\xi_m}{\kappa_{mn}} \hat{\mathbf{x}} - \hat{\mathbf{y}} + \frac{jk_n}{\kappa_{mn}} \hat{\mathbf{z}} \right] \right\} (14)$$

where w is the width of the track, l is the length of the track, y_g = airgap height, and R_{mn} is given by

$$R_{mn} = \frac{\mu_0 \sigma \tau_{mn}}{\kappa_{mn}^2 + \gamma_{mn}^2 + 2\kappa_{mn} \beta_{mn} \coth(\beta_{mn} h)}$$
(15)

$$\kappa_{mn}^2 = \xi_m^2 + k_n^2 \tag{16}$$

$$\xi_m = \frac{2\pi m}{I} \tag{17}$$

$$k_n = \frac{2\pi n}{w} \tag{18}$$

$$\beta_{mn}^2 = \kappa_{mn}^2 - j\mu_0 \sigma \left(P\omega + \xi_m v_x \right) \tag{19}$$

$$\tau_{mn} = \kappa_{mn} v_y + j \left(P \omega + \xi_m v_x \right) \tag{20}$$

The complex harmonic magnitude field source term, S_{mn} , in (14) is determined by evaluating [3, 4]

$$S_{mn} = \frac{1}{lw} \int_{-w/2}^{w/2} \int_{-l/2}^{l/2} B_y^{so}(x, y_g, z, t) e^{-j\xi_m x} e^{-jk_n z} dx dz$$
 (21)

REFERENCES

- [1] J. Bird and T. A. Lipo, "A 3D steady-state magnetic charge finite element model of an electrodynamic wheel," *IEEE Trans. Magn.*, vol. 44, no. 2, pp. 253-265, Feb. 2008.
- [2] J. Bird and T. A. Lipo, "Modeling the 3-D rotational and translational motion of a Halbach rotor above a split-sheet guideway," *IEEE Trans. Magn.*, vol. 45, no. 9, pp. 3233-3242, Sept. 2009.
- [3] S. Paul, "Three-dimensional steady state and transient eddy current modeling," Ph.D. Thesis, Elect. Comp. Eng., Univ. N.C. at Charlotte, Charlotte, NC, 2014.
- [4] S. Paul, W. Bomela, N. Paudel, and J. Z. Bird, "3-D Eddy Current Torque Modeling," *IEEE Trans. Mag.*, vol. 50, no. 2, pp. 905-908, 2014, doi: 10.1109/tmag.2013.2285566.
- [5] C. Bruce et al., "An Electrodynamic Wheel Maglev Vehicle with a Passive U-Guideway," in *Intern. Conf. Elect. Mach. Sys.*, Chiang Mai, Thailand, Nov. 29 - Dec. 2 2022.
- [6] J. Wright and J. Z. Bird, "Analytic damping and stiffness analysis for a 4-DOF electrodynamic wheel maglev vehicle," in 2018 XIII Intern. Conf. Elect. Mach., 2018, pp. 555-561.
- [7] P. Lin, Z. Deng, Z. Ke, W. Lei, X. Wang, and K. Ren, "Dynamic Characteristics and Working Modes of Permanent Magnet Electrodynamic Suspension Vehicle System Based on Six Wheels of Annular Halbach Structure," *Technologies*, vol. 11, no. 1, p. 16, 2023.
- [8] E. P. Furlani, "A two-dimensional analysis for the coupling of magnetic gears," *IEEE Transactions on Magnetics*, vol. 33, no. 3, pp. 2317-2321, 1997
- [9] S. Paul, D. Bobba, N. Paudel, and J. Z. Bird, "Source field modeling in air using magnetic charge sheets," *IEEE Trans. Mag.*, vol. 48, no. 11, pp. 3879-3882, 2012.
- [10] Z. P. Xia, Z. Q. Zhu, and D. Howe, "Analytical magnetic field analysis of halbach magnetized permanent-magnet machines," *IEEE Trans. Magn.*, vol. 40, no. 4, pp. 1864-1872, July 2004.